ChemComm

ROYAL SOCIETY OF CHEMISTRY

COMMUNICATION

View Article Online
View Journal | View Issue

Cite this: *Chem. Commun.*, 2022, **58**, 12708

Received 8th September 2022,
Accepted 20th October 2022

DOI: 10.1039/d2cc04976g

rsc.li/chemcomm

In situ lead oxysalt passivation layer for stable and efficient perovskite solar cells†

Wenjing Hou, *[a] Mengna Guo,[a] Yunzhen Chang,[a] Sheng Zhu,[a] Huan Bi, *[b] Qing Shen, [b] Yaoming Xiao[c] and Gaoyi Han *[a]

A Rb_2SO_4 additive is employed to passivate the Pb^{2+} defects in a perovskite film by forming $PbSO_4$ *in situ*, which can cover the surface and grain boundaries of the perovskite to ensure that the film is not decomposed by moisture. Finally, a device based on the Rb_2SO_4 modification achieved an enhanced power conversion efficiency (22.25%) and long-term stability.

Organic–inorganic halide perovskite solar cells (PSCs) have emerged as potential alternatives to silicon solar cells, and their power conversion efficiency (PCE) has increased from 3.8% to 25.7%.[1–3] However, poor long-term stability is still the key factor hindering their commercialization. Therefore, how to further improve device stability is an urgent topic of investigation.

The quality of the perovskite film is one of the most important factors influencing device PCE and stability.[4] Generally, defects are inevitably introduced in perovskite films due to the rapid crystallization process.[5] These defects can act as an invasion site for water/oxygen or shuttle path for undesirable ion migration.[6] Meanwhile, these defects can act as recombination centres to increase the recombination probability of carriers. Therefore, improving the quality of the perovskite film by passivating defects is an important step for improving device performances.

Additive engineering is of interest because of its simple preparation process and remarkable effect.[7] Additives are mainly divided into organic small molecule additives and inorganic salt additives. Organic small molecule additives have been used to passivate the defects in perovskite based on chemical interactions. Lewis base additives can passivate the under-coordinated Pb^{2+} defects,[8] and Lewis acid additives can passivate the halide defects. Zwitterion additives can passivate the positive and negative defects in perovskite films simultaneously.[9] Although small molecule additives have shown initial success in perovskite solar cells, some small molecule additives have a limited effect in stability improvement of perovskite films and devices, because the bonding strength between the small molecule and the perovskite is generally too weak. In addition, organic small molecule additives have poor thermal stability and are easy to decompose. Therefore, researchers pay more attention to inorganic additives. For example, Li used NaF to passivate both anion and cation vacancy defects because F^- can interact with the organic cation and Pb^{2+} simultaneously.[10] Some researchers also introduced RbI into perovskite precursor solutions and found that Rb^+ can act as an A-site cation to improve the efficiency and stability of the device by making the energy levels more closely matched and passivating the defects.[2,11,12] Unlike organic small molecules, inorganic oxides or nitrides are often chosen to passivate the structural defects and protect silicon from degradation in silicon-based solar cells, because they are compact and chemically stable. This provides the inspiration for the defect passivation of perovskite solar cells.

Considering that the perovskite film may contain under-coordinated Pb^{2+} defects, SO_4^{2-} was introduced to passivate the uncoordinated Pb^{2+} defects. The interaction between SO_4^{2-} and Pb^{2+} can retard the nucleation rate of the perovskite, which is favorable to increasing the grain size and reducing pinholes. In order to reduce the interference by the impurity cation, Rb^+ was chosen as the corresponding cation due to its positive influence on device performances. Therefore, the inorganic rubidium sulphate (Rb_2SO_4) additive is added to the perovskite precursor solution to form $PbSO_4$ *in situ*, which can cover the surface and grain boundaries of the perovskite and passivate the Pb defects in the perovskite film. In addition, Rb^+ in Rb_2SO_4 can passivate the iodine defects. Due to the defect passivation role of the

[a] *Institute of Molecular Science, Key Laboratory of Chemical Biology and Molecular Engineering of Education Ministry, Key Laboratory of Materials for Energy Conversion and Storage of Shanxi Province, Shanxi University, Taiyuan 030006, P. R. China. E-mail: han_gaoyis@sxu.edu.cn, wjhou2016@sohu.com*

[b] *Faculty of Informatics and Engineering, The University of Electro-Communications, 1-5-1 Chofugaoka, Chofu, Tokyo 182-8585, Japan. E-mail: hbi.trans.sci@uec.ac.jp*

[c] *College of Chemical Engineering and Materials Science, Quanzhou Normal University, Quanzhou 362000, P. R. China*

† Electronic supplementary information (ESI) available: Experimental procedures, device fabrication details and characterization. See DOI: https://doi.org/10.1039/d2cc04976g

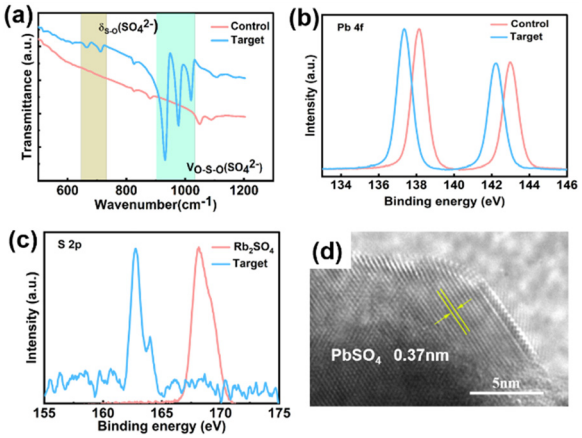

Fig. 1 (a) FTIR spectra of the perovskite film; XPS spectra of (b) Pb 4f for control and target perovskite films; (c) S 2p for Rb_2SO_4 and the target perovskite film; (d) TEM image of the perovskite film with Rb_2SO_4 additive.

Rb_2SO_4 additive, the PCE of devices increased from 20.62% to 22.25%, and photocurrent hysteresis was inhibited significantly. This is mainly attributed to the improvement of the quality of the perovskite film and reduction of nonradiative recombination. In addition, the efficiency of the unencapsulated control device degraded to 70% of the initial efficiency after aging in air conditions with 15–20% relative humidity for 500 h, while the efficiency of the target device with the Rb_2SO_4 additive only degraded to 82% of the initial efficiency.

As shown in Fig. S1 (ESI†), a $Rb_{0.02}(FA_{0.95}Cs_{0.05})_{0.98}Pb(I_{0.97}Br_{0.01}Cl_{0.02})_3$ perovskite film modified with different concentrations of Rb_2SO_4 additive was coated on SnO_2 films. Fourier transform infrared spectroscopy (FTIR) and X-ray photoelectron spectroscopy (XPS) measurements were performed to evaluate potential chemical relationships between the perovskite and Rb_2SO_4. As shown in Fig. 1a, some new peaks are clearly observed in the target films. The peak located around 665 cm^{-1} is the symmetric and asymmetric bending ($\delta_{S-O}(SO_4)$) of the S–O bond. Another peak situated near 980 cm^{-1} is the symmetric stretching vibration ($\nu_{S-O}(SO_4)$) of the S–O bond,[7] which supports that SO_4^{2-} is present in the target perovskite films. Fig. S2 (ESI†) shows the full XPS spectrum of the target film. As shown in Fig. 1b, after introducing Rb_2SO_4, the binding energy of the Pb $4f_{7/2}$ (138.72 eV) and Pb $4f_{5/2}$ (143.59 eV) states in the control perovskite films moved to 137.81 eV and 142.67 eV,[13] respectively. Meanwhile, compared with Rb_2SO_4, the binding energy of S 2p in the target perovskite films reduced from 168.70 eV to 162.80 eV (Fig. 1c).[13] The I 3d peaks shifted toward lower binding energy by 0.20 eV, mainly because the Rb^+ can passivate the iodine defects (Fig. S3, ESI†).[14] These results indicate that there is a strong chemical interaction between Rb_2SO_4 and the perovskite. The results of high-resolution transmission electron microscopy (HRTEM) in Fig. 1d indicated that the perovskite is surrounded by substances with good crystallinity. According to PDF #89-3750, the lattice spacing of 0.37 nm corresponds to the (111) crystal plane of $PbSO_4$,[13] which illustrates that the Rb_2SO_4 additive can react with Pb^{2+} to form a thin continuous $PbSO_4$ layer on the surface of the perovskite, which is conducive to passivating the uncoordinated Pb^{2+} defects. And the TEM of the precursor solution in Fig. S4 (ESI†) indicates that $PbSO_4$ has formed in the precursor solution, which has also been verified by previous work.[5]

As shown in Fig. S5 and S6 (ESI†) and Fig. 2a and b, the grain size in the perovskite film increases from 1.39 μm to 1.58 μm and the number of pinholes decreases obviously with increasing the Rb_2SO_4 concentration from 0.00 to 0.20 mg mL^{-1}. And the target film with 0.20 mg mL^{-1} Rb_2SO_4 exhibited a decrease in roughness from 38.2 nm to 30.5 nm. The improved film quality is mainly due to the uncoordinated Pb^{2+} defects being passivated by SO_4^{2-} and the iodine defects being passivated by Rb^+ in Rb_2SO_4. In addition, the *in situ* reaction between SO_4^{2-} and Pb^{2+} is favorable to retarding the nucleation rate of the perovskite, leading to the increased grain size and reduced pinhole number.[5] However, when the concentration increased to 0.30 mg mL^{-1}, the grain size decreased, causing an increase in grain boundary defects.

Fig. 2c and d show the cross-sectional view SEM images of perovskite films with and without Rb_2SO_4 modification. The thickness of the perovskite film increased from 501 nm to 525 nm after Rb_2SO_4 modification. In Fig. S7 (ESI†), the light absorption intensity of the target perovskite films at 510–660 nm was stronger than that of the control perovskite film, which was mainly due to the improved film morphology. The XRD patterns of perovskite films in Fig. S8 (ESI†) indicate that the Rb_2SO_4 will not influence the composition of the perovskite.

We further quantified the defect density of perovskite films by the space charge limited current (SCLC) technique. Fig. S9a and b (ESI†) show the dark *I–V* curves of the control and target devices (ITO/Perovskite without or with Rb_2SO_4/Au). The defect density of perovskite films can be calculated according to eqn (1):[2]

$$n_t = \frac{2\varepsilon\varepsilon_0 V_{TFL}}{eL^2} \quad (1)$$

where ε_0 is the vacuum dielectric constant, ε is the dielectric constant of the perovskite, V_{TFL} is the limit voltage of trap filling, e is the basic charge, and L is the thickness of the perovskite film. V_{TFL} decreased from 0.92 V for the control perovskite film to 0.63 V for the target perovskite film. A lower defect density was obtained for the optimized device

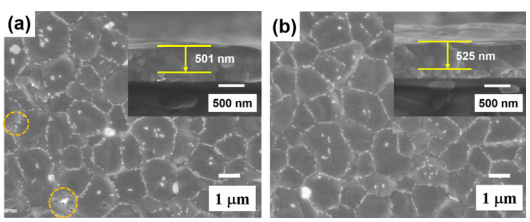

Fig. 2 Top-view and cross-sectional SEM images of the (a) control and (b) target perovskite films deposited on SnO_2.

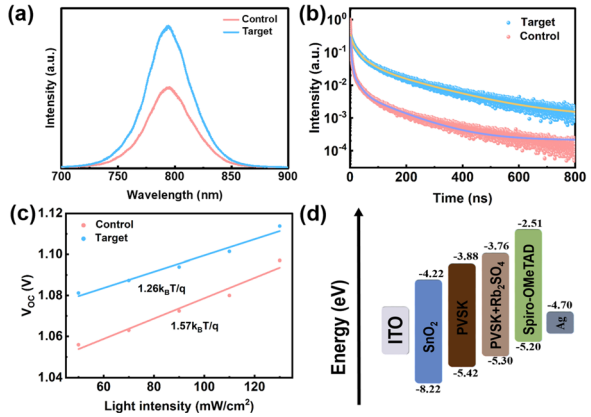

Fig. 3 (a) PL and (b) TRPL of the perovskite films deposited on glass. (c) V_{OC} dependence on light intensity, and (d) energy level diagram.

(4.95×10^{15} cm^{-3}) compared with the control perovskite film (7.96×10^{15} cm^{-3}).

According to the steady-state photoluminescence (PL) spectra shown in Fig. 3a and Fig. S10 (ESI†), compared with the control perovskite films, the target film with 0.20 mg mL^{-1} Rb_2SO_4 modification shows higher PL intensity and a slight shift from 795.10 nm to 794.45 nm, which indicates the reduced non-radiative recombination caused by Rb_2SO_4. However, when the concentration of Rb_2SO_4 increased to 0.30 mg mL^{-1}, the peak intensity decreased relatively.

Fig. 3b shows the time-resolved photoluminescence (TRPL) spectra; the average carrier lifetime (τ_{ave}) can be calculated according to eqn (2) and (3)[2]

$$I(t) = I_0 + A_1 \exp(-t/\tau_1) + A_2 \exp(-t/\tau_2) \quad (2)$$

$$\tau_{ave} = \frac{A_1\tau_1^2 + A_2\tau_2^2}{A_1\tau_1 + A_2\tau_2} \quad (3)$$

The decay lifetime is divided into two parts, namely a fast (τ_1) process and a slow (τ_2) process. Table S1 (ESI†) shows that the τ_{ave} of the target perovskite film (127.51 ns) was longer than that of the control perovskite film (75.40 ns). The enhanced PL intensity and the extended average lifetime indicate the decreased non-radiative recombination.[5] In Fig. S11 (ESI†), the dependence curve of J_{SC} on light intensity follows the equation: $J_{SC} \propto I^a$. The a of the target device is closer to 1 than that of the control device. In Fig. 3c, V_{OC} and light intensity follow (4):[2]

$$V_{OC} = \frac{nk_BT}{q}\ln\left(\frac{J_{SC}}{J_0}\right) \quad (4)$$

where n is the ideality factor that can be obtained from the slope, k_B is the Boltzmann constant, T is the temperature, and q is the elemental charge. $n = 1$ indicates a trap-free condition. It is found that n decreases from 1.57 for the control device to 1.26 for the target device, which means that the non-radiative recombination of the film is inhibited. According to the results of the Tauc plot and ultraviolet photoelectron spectroscopy in Fig. S12 and S13 (ESI†) and Table S2 (ESI†), the Valence Band Maximum (VBM) of the control and target perovskites was −5.42 eV and −5.30 eV, respectively. The shift of the valence band makes the energy level of the perovskite absorption layer match that of the hole transport layer more closely (Fig. 3d), which is beneficial to extracting holes and reducing carrier recombination.[12] Moreover, the matched energy level explains the significant enhancement of V_{OC} after Rb_2SO_4 additive modification.[12,15] The Mott–Schottky curves of the control and target are shown in Fig. S14 (ESI†); the built-in potentials (V_{bi}) of the control device and target device are 0.82 V and 0.87 V, respectively. The increased V_{bi} is beneficial to the separation of photogenerated charge and inhibits carrier recombination.[2] Electrochemical impedance spectroscopy (EIS) was measured to further explore the carrier recombination as shown in Fig. S15 (ESI†). A lower charge transfer resistance (R_{ct}) indicates a higher charge transfer capability.[16] At the same time, the recombination resistance (R_{rec}) increased, which indicates that the Rb_2SO_4 additive can reduce the possibility of carrier recombination. Fig. S16 (ESI†) shows J–V curves of devices under dark conditions. After adding Rb_2SO_4 into the perovskite, the decreased saturation current density value means that the higher coverage of the perovskite.

The influences of Rb_2SO_4 content on device performances were investigated as shown in Fig. S17 and S18 (ESI†) and Table S3 (ESI†). All photovoltaic parameters increased with the increase in Rb_2SO_4 concentration and reached the maximum value at 0.20 mg mL^{-1}. However, when the concentration increases to 0.30 mg L^{-1}, the device performance decreases. This is mainly because the decreased grain size can lead to an increase in the number of grain boundaries, resulting in increased recombination possibility. As shown in Fig. 4a and Table S4 (ESI†), the control device produced a PCE of 20.62% in the forward scan (FS) with a V_{OC} of 1.08 V, a J_{SC} of 25.06 mA cm^{-2}, and a FF of 76.17%, and a PCE of 20.15% in the reverse scan (RS) with a V_{OC} of 1.07 V, a J_{SC} of 25.27 mA cm^{-2}, and a FF of 74.52%. By contrast, the target device of the perovskite with Rb_2SO_4 modification delivered the highest

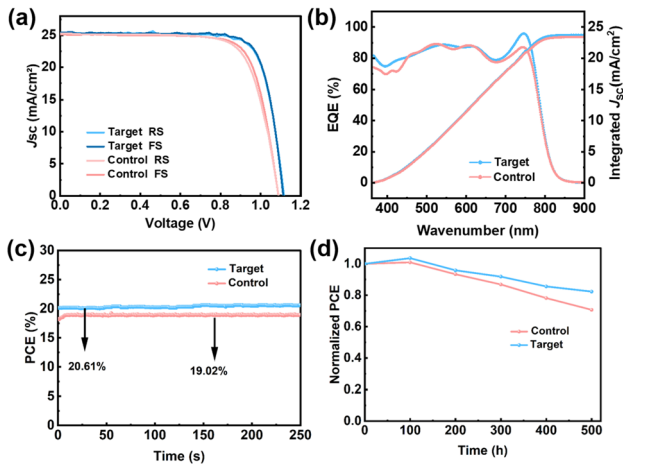

Fig. 4 (a) Reverse and forward scanned J–V curves of devices. (b) IPCE and integrated J_{SC} of devices. (c) The PCE at the maximum power point for the devices. (d) PCE *versus* time for the unencapsulated devices aged in the air with relative humidity of 15–20% RH in the dark at room temperature.

PCE of 22.25% in the forward scan (FS) with a V_{OC} of 1.11 V, a J_{SC} of 25.39 mA cm^{-2}, and a FF of 78.95%, and a PCE of 22.10% in the reverse scan (RS) with a V_{OC} of 1.12 V, a J_{SC} of 25.43 mA cm^{-2}, and a FF of 77.59%. The increased J_{SC} can be attributed to the improved light-harvesting. As Fig. S19 (ESI†) shows, the main reasons for the higher FF than the control device is reduced non-radiative recombination, rather than charge transfer loss.[17,18] The V_{OC} is influenced not only by defect-related non-radiative recombination, but also by the energy band mismatch caused by Rb_2SO_4.[18,19] The performance statistics results of 20 devices shown in Fig. S20 (ESI†) and Table S5 (ESI†) indicate that the control devices and the target devices both show good reproducibility and the average PCE of the target device (21.52%) is better than that of the control device (19.90%). For the control and target devices, the integrated J_{SC} of the external quantum efficiency (EQE) were 23.41 and 23.74 mA cm^{-2}, respectively (Fig. 4b).

In addition, we tested the steady-state current density and PCE at the maximum power point as shown in Fig. 4c and Fig. S21 (ESI†). The control device delivered a stable PCE of 19.02% with a stable output current density of 21.37 mA cm^{-2} at 0.89 V, whereas the target device delivered a stable PCE of 20.61% with a stable output current density of 22.90 mA cm^{-2} biased at 0.9 V after the same time. Finally, we performed long-term stability tests for unencapsulated devices under ambient conditions at a relative humidity of 15–20% and a temperature of 20 °C, as shown in Fig. 4d and Fig. S22 (ESI†). After 500 h of exposure to the air, the target device and control device retained 82% and 70% of their initial PCE, respectively. The PCE attenuation is mainly caused by the decreased V_{OC} and FF. These results benefit from moderate amounts of the Rb_2SO_4 additive prolonging the carrier lifetime, inhibiting the nonradiative recombination of carriers, and improving the quality of the perovskite film. The quality of the perovskite film is the key factor affecting the device stability. Therefore, we evaluated the long-term stability of the perovskite film in Fig. S23 (ESI†). The perovskite films were placed in an environment of 50–60% relative humidity to observe the decomposition of the perovskite. The results showed that after 5 days of aging, the unmodified perovskite film decomposed quickly, while the Rb_2SO_4 modified perovskite film remained black. The formation of an *in situ* passivation layer is the main reason for the improvement of humidity stability. The results in Fig. S24 and S25 (ESI†) also verified that the improved stability of the perovskite film is partly due to using the chlorobenzene anti-solvent.[20]

In summary, we systematically investigated the passivation effect of Rb_2SO_4 on the uncoordinated Pb defects of perovskite films by adding Rb_2SO_4 to a perovskite precursor solution. We found that SO_4^{2-} in Rb_2SO_4 reacted with uncoordinated Pb^{2+} to form a $PbSO_4$ passivation layer and Rb^+ in Rb_2SO_4 can passivate iodine defects, which can improve the quality of the perovskite films, prolong carrier lifetime and decrease defect density. The PSCs with the Rb_2SO_4 additive achieved a PCE of 22.25% without obvious photocurrent hysteresis. The unencapsulated device with the Rb_2SO_4 additive showed remarkably enhanced long-term stability, retaining 82% of its original PCE after aging for 500 h. Therefore, Rb_2SO_4 is an effective additive to improve the photovoltaic performance and long-term stability of devices.

This work was financially supported by the National Natural Science Foundation of China (U21A20172, 61804091, and U21A6004). We are grateful for the Fujian Natural Science Funds for Distinguished Young Scholars (2020J06046).

Conflicts of interest

There are no conflicts to declare.

Notes and references

1 NREL, Best Research-Cell Efficiency Chart, https://www.nrel.gov/pv/cell-efficiency.html.
2 H. Bi, G. Han, M. Guo, C. Ding, S. Hayase, H. Zou, Q. Shen, Y. Guo and W. Hou, *Sol. RRL*, 2022, 2200352.
3 Z. Xing, S. Li and S. Yang, *Small Struct.*, 2022, **3**, 2200012.
4 S. Chen, S. Zhang and Q. Zheng, *Sci. China Mater.*, 2020, **63**, 719–727.
5 X. Ma, L. Yang, X. Shang, M. Li, D. Gao, C. Wu, S. Zheng, B. Zhang, J. Chen, C. Chen and H. Song, *Chem. Eng. J.*, 2021, **426**, 130685.
6 S. Yang, S. Chen, E. Mosconi, Y. Fang, X. Xiao, C. Wang, Y. Zhou, Z. Yu, J. Zhao, Y. Gao, F. Angelis and J. Huang, *Science*, 2019, **365**, 473–478.
7 C. Zhang, H. Wang, H. Li, Q. Zhuang, C. Gong, X. Hu, W. Cai, S. Zhao, J. Chen and Z. Zang, *J. Energy Chem.*, 2021, **63**, 452–460.
8 N. Saykar, A. Arya and S. Mahapatra, *J. Phys. D: Appl. Phys.*, 2022, **55**, 043001.
9 S. Liu, Y. Guan, Y. Sheng, Y. Hu, Y. Rong, A. Mei and H. Han, *Adv. Energy Mater.*, 2019, 1902492.
10 N. Li, S. Tao, Y. Chen, X. Niu, C. Onwudinanti, C. Hu, Z. Qiu, Z. Xu, G. Zheng, L. Wang, Y. Zhang, L. Li, H. Liu, Y. Lun, J. Hong, X. Wang, Y. Liu, H. Xie, Y. Gao, Y. Bai, S. Yang, G. Brocks, Q. Chen and H. Zhou, *Nat. Energy*, 2019, **4**, 408–415.
11 B. Liu, H. Bi, D. He, L. Bai, W. Wang, H. Yuan, Q. Song, P. Su, Z. Zang, T. Zhou and J. Chen, *ACS Energy Lett.*, 2021, **6**, 2526–2538.
12 S. Sahamir, M. Kamarudin, T. Ripolles, A. Baranwal, G. Kapil, Q. Shen, H. Segawa, J. Bisquert and S. Hayase, *J. Phys. Chem. Lett.*, 2022, **13**, 3130–3137.
13 W. Wang, Q. Zhou, D. He, B. Liu, L. Bai, C. Xu, Q. Song, P. Zhao, C. Chen, K. Sun, H. Yang, Z. Zang, D. Lee and J. Chen, *Sol. RRL*, 2022, **6**, 2100893.
14 C. Xu, X. Chen, S. Ma, M. Shi, S. Zhang, Z. Xiong, W. Fan, H. Si, H. Wu, Z. Zhang, Q. Liao, W. Yin, Z. Kang and Y. Zhang, *Adv. Mater.*, 2022, **34**, 2109998.
15 D. Prochowicz, M. Tavakoli, A. Kalam, R. Chavan, S. Trivedi, M. Kumarh and P. Yadav, *J. Mater. Chem. A*, 2019, **7**, 8218–8225.
16 M. Hao, H. Wang, Y. Wang, Y. Qin, J. Zhang and X. Ai, *J. Power Sources*, 2020, **479**, 229077.
17 B. Qi and J. Wang, *Phys. Chem. Chem. Phys.*, 2013, **15**, 8972–8982.
18 P. Chen, Y. Bai and L. Wang, *Small Struct.*, 2021, **2**, 2000050.
19 P. Zhang, F. Cao, W. Tian and L. Li, *Sci. China Mater.*, 2022, **65**, 321–327.
20 M. Xiao, F. Huang, W. Huang, Y. Dkhissi, Y. Zhu, J. Etheridge, A. Gray-Weale, U. Bach, Y. Cheng and L. Spiccia, *Angew. Chem., Int. Ed.*, 2014, **53**, 9898–9903.